

Surface core-level shifts and electronic structures of Yb compounds studied with use of photoemission spectroscopy

En-Jin Cho, J.-S. Chung, and S.-J. Oh*

Department of Physics, Seoul National University, Seoul 151-742, Korea

S. Suga,[†] M. Taniguchi,[‡] and A. Kakizaki

Synchrotron Radiation Laboratory, Institute for Solid State Physics, University of Tokyo, Tanashi, Tokyo 188, Japan

A. Fujimori[§]

National Institute for Research in Inorganic Materials, Tsukuba, Ibaraki 305, Japan

H. Kato and T. Miyahara

Photon Factory, National Laboratory for High Energy Physics, Oho, Tsukuba, Ibaraki 305, Japan

T. Suzuki and T. Kasuya

Department of Physics, Faculty of Science, Tohoku University, Sendai 980, Japan

(Received 9 September 1992)

Mixed-valent Yb compounds (YbIn₂, Yb₄As₃, YbCu₂, YbAl₃, Yb₄Sb₃, Yb₄Bi₃) and divalent YbPb₃ were studied by high-resolution photoemission spectroscopy with the use of synchrotron radiation in the photon energy range $40 \leq \hbar\omega \leq 140$ eV. It was found that the divalent $4f$ spectra in all of these compounds consist of two components, one from the bulk and the other from the surface layer(s). The surface components are shifted to higher binding energies by 0.52–0.94 eV. These surface core-level shifts are reasonably well described by the Johansson and Mårtensson fully screened core-hole model with Miedema's empirical scheme for cohesive energy estimation. The $4d$ or $5d$ core levels of some anion atoms are also observed to be shifted at the surface to the higher binding energies by 0.36–0.56 eV, suggesting that the charge transfer between cation and anion atoms is not the origin of surface core-level shifts in these compounds. The electron mean free path is found to decrease with decreasing kinetic energies of the photoelectron down to $\hbar\omega = 40$ eV in these compounds. The bulk Yb valence ν and the $4f$ level binding energy ϵ_f for each compound are also deduced from the *bulk* $4f$ spectral features. The zero-temperature magnetic susceptibility $\chi(0)$ estimated using the lowest-order analytic relation for the Anderson impurity Hamiltonian from these values is in good agreement with available experimental data, suggesting that the Anderson impurity Hamiltonian description is a good starting point for the electronic structures of these Yb compounds. The hybridization strength Δ between the $4f$ level and conduction electrons is found to be in the range of 17–78 meV.

I. INTRODUCTION

Intermetallic rare-earth compounds are interesting because they often show anomalous physical phenomena such as mixed-valency¹ or heavy-fermion properties² due to the interaction between localized $4f$ electron and delocalized conduction electrons. Many theoretical and experimental investigations have been performed to understand the origin of these anomalous physical properties. Electron spectroscopic techniques, such as photoemission spectroscopy (PES) and bremsstrahlung isochromat spectroscopy (BIS) are powerful tools to study electronic structures experimentally, and these techniques revealed important informations on this interesting class of materials. For example, a systematic study on the $4f$ spectral weight of Ce compounds by PES and BIS showed that the Anderson impurity Hamiltonian gives a good description of their electronic structures,³ and the equilibrium properties such as magnetic susceptibility and the excitation properties such as PES can be understood

within the same framework.⁴ Although this picture was quite successful in explaining physical properties of many Ce compounds, no such systematic study has yet been performed on other rare-earth compounds. In this paper, we report photoemission spectroscopy study on the valence-band region of several mixed-valent (YbIn₂, Yb₄As₃, YbCu₂, YbAl₃, Yb₄Sb₃, Yb₄Bi₃) and divalent (YbPb₃) Yb compounds using synchrotron radiation light in the photon energy range $40 \leq \hbar\omega \leq 140$ eV. Yb compounds are particularly interesting because the electron-hole symmetry exists between Ce and Yb compounds so that the theoretical formalisms used for Ce compounds can be directly applied to the Yb case by simply interchanging the role of the $4f$ electron with that of the $4f$ hole. Hence valence-band photoemission spectra, especially the $4f$ electron spectral weights, are expected to be very useful in understanding the electronic structures of Yb compounds as in the case of Ce compounds.³

In all of the valence-band spectra of Yb compounds we studied, we found strong contributions from surface lay-

ers in the form of the surface shifted $4f$ peaks. Since this surface contribution will influence the determination of the bulk electronic structures,⁵ it is important to separate out the bulk and surface peaks accurately. Furthermore, although the surface core-level shifts (SCS) have been observed for many rare-earth metals and compounds,^{6–19} the proper understanding of the magnitude and the sign of SCS is still lacking.^{20–23} At least three different models have been proposed for the origin of SCS. Johansson and Mårtensson²⁰ proposed based on their fully screened core-hole model that SCS results from the difference of cohesive energies between the surface and the bulk. In this model, the final-state relaxation (screening) of the core hole is an important factor in determining SCS. Citrin and Wertheim,²¹ on the other hand, discussed SCS qualitatively in terms of the narrowing density of states of surface atoms relative to that of the bulk, and proposed that the SCS is predominantly an initial-state effect. Davenport *et al.*²² and Priester, Allan, and Lannoo²³ proposed yet another mechanism based on the charge transfer between the cation and anion atoms and the resulting Madelung potential difference between the surface and the bulk, which was applied mainly to explain SCS's in III-V semiconductors.^{24–26} Clearly it is interesting to see which of these models is more appropriate in describing the surface core-level shifts of these Yb compounds.

For these purposes, we first determined the magnitude and the sign of the $4f$ SCS for each Yb compound systematically by fitting the valence-band photoemission spectra at several photon energies with two peaks, one from the bulk and the other from the surface-shifted $4f$ levels. By analyzing the spectra at several different photon energies systematically, we minimized the arbitrariness in the fitting procedure and were able to check for self-consistency. The anion core levels were also analyzed for possible surface contributions. We then compared the value of SCS and the bulk $4f$ level position of each compound with the predictions of the Johansson and Mårtensson's fully screened core-hole model using Miedema's empirical scheme for cohesive energy estimation. Finally we deduced the electron mean free path of the $4f$ photoelectron as a function of the electron kinetic energy from the intensity ratios of the bulk and the surface peaks, and compared with different theoretical models. For some of the Yb compounds studied here the valence-band photoemission spectra were already published and SCS's were identified,^{16,18,19} but in this paper we supplement these studies with higher-resolution data and by analyzing the spectra at several different photon energies to check the consistency of the data analyses and to see the trend of the electron mean free path as a function of the kinetic energy.

Having identified the bulk and surface features in the $4f$ spectra, we were able to determine the bulk valence v and the bulk $4f$ level binding energy ϵ_f of these Yb compounds. These were then used to estimate the zero-temperature magnetic susceptibility $\chi(0)$ using the analytic relation valid for the Anderson impurity Hamiltonian in the $U \rightarrow \infty$ limit, which was compared with the experimental data when available. This is to see whether the Anderson impurity Hamiltonian can describe the

low-energy and high-energy properties of Yb compounds consistently, as in the case of Ce compounds.³ The hybridization strengths Δ between the $4f$ level and conduction electrons were also deduced from the bulk $4f$ spectral weight for each compound, and compared with those for typical Ce compounds.

The organization of this paper is as follows. In Sec. II, the experimental details are discussed. In Sec. III, the data analysis procedure is explained in detail, and the results of the fit for the Yb $4f$ and anion core-level spectra are described. In Sec. IV, the bulk $4f$ level binding-energy position and the surface core-level shift of each compound are compared with the predictions of Johansson and Mårtensson's fully screened core-hole model, and the change of the electron mean free path as a function of the kinetic energy is determined. The bulk Anderson Hamiltonian parameters of these Yb compounds are also deduced, and compared with the magnetic susceptibility data. Section V concludes the paper.

II. EXPERIMENT

The samples we studied are YbPb₃, YbIn₂, YbCu₂, YbAl₃, Yb₄As₃, Yb₄Sb₃, and Yb₄Bi₃. Polycrystalline ingots of YbPb₃, YbIn₂, YbCu₂, and YbAl₃ were grown in the vacuum furnace with tungsten heater, where appropriate amounts of elements were sealed inside the tungsten crucible vacuum welded by the electron beam. Single crystals of Yb₄As₃, Yb₄Sb₃, and Yb₄Bi₃ were grown in the vacuum furnace with SiC heater, where they were sealed in the quartz tube with alumina boat. These samples were annealed after growth, and their crystal structures and stoichiometry were checked by the x-ray analysis. Fresh surfaces for photoemission spectroscopy measurements were obtained by fracturing or scraping the sample *in situ*. Valence-band photoemission spectra were measured using soft x-ray synchrotron radiation on the Beam Line 11-D of Photon Factory in Japan, equipped with CDM (constant deviation monochromator)²⁷ and DCMA (double pass cylindrical analyzer). Oxygen and carbon contaminations were monitored during measurements, and when they were found to be nonnegligible the spectra were discarded and samples were scraped again. The base pressure of the analysis chamber was usually 3×10^{-10} torr, and because of this relatively poor vacuum, we had to scrape one sample several times. However, the spectra analyzed in this paper are from clean surfaces only.

III. DATA ANALYSES AND RESULTS

A. Yb $4f$ spectra

Figure 1 shows typical valence-band photoemission spectra of Yb compounds (YbPb₃, YbIn₂, Yb₄As₃, YbCu₂, YbAl₃, Yb₄Sb₃, Yb₄Bi₃) taken with the soft x-ray photons from the synchrotron radiation source. In this photon energy range, the valence-band spectra near the Fermi level of these compounds are dominated by the Yb $4f$ emissions due to the atomic cross section differences, except for YbCu₂ case [Fig. 1(d)] where Cu $3d$ emission is also strong. For each sample, photoemission spectra

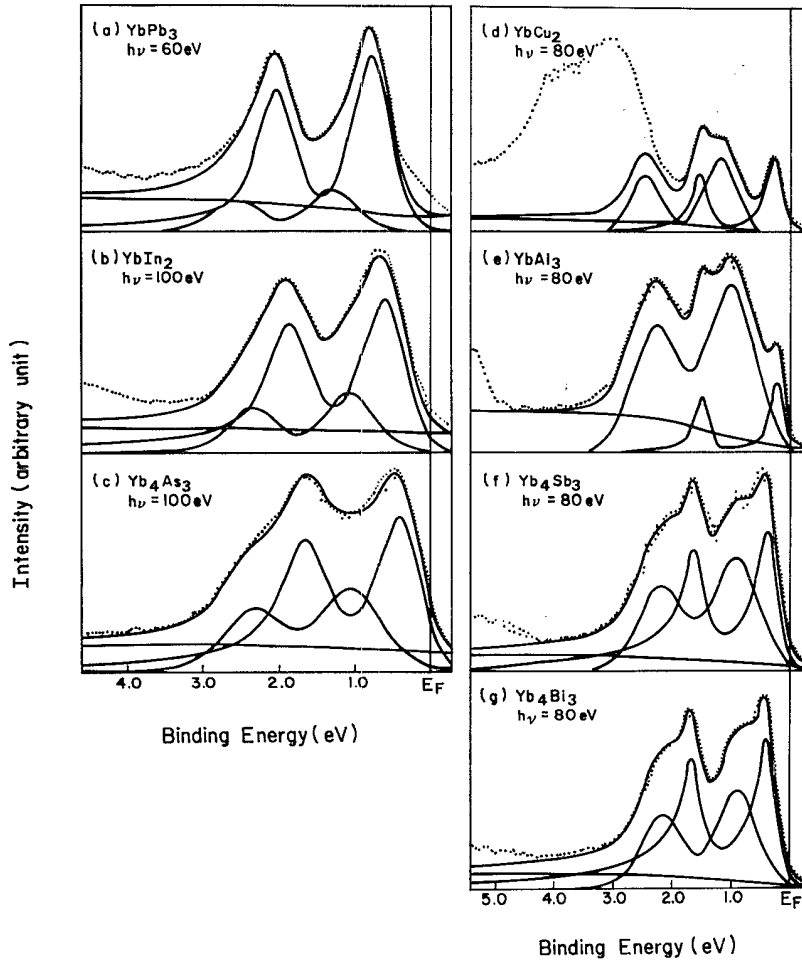


FIG. 1. Valence-band photoemission spectra of (a) YbPb₃, (b) YbIn₂, (c) Yb₄As₃, (d) YbCu₂, (e) YbAl₃, (f) Yb₄Sb₃, and (g) Yb₄Bi₃ using synchrotron radiation (dots) and their fit with the bulk and the surface 4*f* spin-orbit pairs (solid lines). The higher binding-energy peak represents the emission from the surface. Backgrounds due to inelastic electrons are also shown.

were taken usually at $\hbar\omega=40, 60, 80, 100, 120,$ and 140 eV. To obtain informations on the surface shifted 4*f* peaks, we deconvoluted the experimental raw data by curve fitting procedures with two sets of Yb 4*f* spin-orbit doublets 4*f*_{5/2} and 4*f*_{7/2}, one set for the bulk and the other for the surface. The result of the fit is shown in the figure with solid line, while dots represent raw data. The spectrum of YbCu₂ in Fig. 1(d) is only partially fitted because of the strong contribution from Cu 3*d* emissions.¹⁶ The intensity ratio between 4*f*_{5/2} and 4*f*_{7/2} peaks in each doublet is fixed as their degeneracy ratio 0.75, and the energy separation between two peaks was set $\epsilon_{f_{5/2}} - \epsilon_{f_{7/2}} = 1.27 \pm 0.02$ eV, consistent with the atomic spin-orbit energy 1.27 eV.

Each theoretical peak is represented by the Mahan line shape²⁸

$$I(\omega) = \int_0^\infty \frac{\gamma/\pi}{(\omega-\omega')^2 + \gamma^2} \frac{1}{\Gamma(\alpha)\omega'} \left[\frac{\omega'}{Gzy} \right]^\alpha \times \exp \left[-\frac{\omega'}{Gzy} \right] d\omega',$$

where $\Gamma(\alpha)$ is the gamma function and other symbols will be explained below. This line shape represents the convolution between the intrinsic lifetime Lorentzian broaden-

ing of the 4*f* core hole $\gamma/\pi/(\omega^2 + \gamma^2)$ and excitonic many-body effects^{28,29} resulting from interactions between the core-hole and conduction electron states ($[\theta(\omega)/\Gamma(\alpha)\omega](\omega/Gzy)^\alpha \exp(-\omega/Gzy)$), where Gzy is the Mahan cutoff parameter (band width) which we set 6.0 eV here, α is the asymmetry parameter, and $\theta(\omega)$ is the step function. The Lorentzian broadening 2γ [full width at half maximum (FWHM)] due to the 4*f* core-hole lifetime is found through the curve-fitting process and its value of each compound is listed in the fifth column of Table I. The values of 2γ in YbPb₃, YbIn₂, YbCu₂, and YbAl₃ are near 0.15 eV and comparable to earlier results,^{16,18} but those in Yb₄As₃, Yb₄Sb₃, and Yb₄Bi₃ are about 0.24 eV and considerably larger as pointed out previously.¹⁹ This may be due to the increased hybridization strength³⁰ in the latter compounds (see Sec. IV D below).

To take into account the spectral broadening due to the instrumental resolution, we convolute this Mahan line shape with the Gaussian function of the half-width Γ . There are two factors that affect the instrumental resolution; one is the photon energy broadening from the CDM monochromator Γ_{mono} [half width at half maximum (HWHM)] and the other is the resolution of the electron energy analyzer DCMA Γ_{pass} (HWHM). The total Gaussian broadening Γ (HWHM) can be written as $(\Gamma_{\text{mono}}^2 + \Gamma_{\text{pass}}^2)^{1/2}$. The values for Γ (HWHM) used in the

curve fitting of the bulk $4f$ peaks are calculated from the theoretical estimates on Γ_{mono} and Γ_{pass} for each experimental setting. However, in order to obtain better results, we allowed the variation of the Γ (HWHM) value up to 20% from the theoretical one in the curve-fitting process. This variation is in considerations of possible errors in theoretical estimates on Γ_{mono} and Γ_{pass} and other experimental uncertainties. However, when the same experimental settings were used to measure several spectra, we used the same value of Γ in their analysis. The Γ values for the surface peaks are allowed to be much larger than those of the bulk in order to take into account the facts that (i) more than one surface layer may contrib-

ute with different binding energies and (ii) surfaces of different crystallographic orientations may have different SCS values. The Gaussian broadenings Γ used in the actual curve fittings are shown in the third column of Table I. The background due to the inelastically scattered electrons is subtracted from the raw data by assuming that the amount of the background $B(\epsilon)$ at the electron kinetic energy ϵ is proportional to the integrated total intensity above this kinetic energy, i.e.,

$$B(\epsilon) = \beta \int_{\epsilon_0}^{\epsilon} f(\epsilon') d\epsilon'.$$

The value of the proportional constant β is also taken as

TABLE I. Summary of the results from the analyses of the Yb $4f$ photoemission spectra at different photon energies: 2Γ (FWHM) is the Gaussian broadening, β is the proportional constant of the background, 2γ (FWHM) is the intrinsic lifetime of the $4f$ core level (Lorentzian broadening), I_S/I_B is the intensity ratio of the surface peak relative to the bulk peak, α is the asymmetry parameter, $\epsilon_{f_{7/2}}^B$ is the $4f_{7/2}$ level binding energy of the bulk and $\Delta E = \epsilon_{f_{7/2}}^S - \epsilon_{f_{7/2}}^B$ is the surface core-level energy shift. B and S denote the bulk and the surface components, respectively. Estimated error bars are given in parentheses in units of the last digit.

Compound	Photon energy (eV)	2Γ (eV)		β		2γ (eV)	$\frac{I_S(+2)}{I_B(+2)}$	α		$\epsilon_{f_{7/2}}^B$ (eV)	$\Delta E = \epsilon_{f_{7/2}}^S - \epsilon_{f_{7/2}}^B$ (eV)
		B	S	B	S			B	S		
YbPb ₃	40	0.40	0.63	0.050	0.00	0.14(8)	0.268	0.10	0.00	0.70(3)	0.54(2)
	60	0.46	0.63	0.080	0.00		0.235				
	80	0.60	0.63	0.080	0.00		0.171				
	100	0.50	0.63	0.080	0.00		0.171				
	120	0.58	0.63	0.080	0.00		0.0431				
YbIn ₂	40	0.40	0.66	0.020	0.00	0.18(8)	0.974	0.15	0.00	0.55(3)	0.52(2)
	60	0.46	0.66	0.020	0.00		0.796				
	80	0.60	0.66	0.020	0.00		0.593				
	100	0.50	0.66	0.020	0.00		0.361				
	140	0.50	0.66	0.020	0.00		0.220				
Yb ₄ As ₃	60	0.46	0.86	0.040	0.00	0.24(8)	0.909	0.15	0.00	0.30(3)	0.70(2)
	80	0.46	0.88	0.040	0.00		0.770				
	100	0.50	0.80	0.040	0.00		0.562				
	120	0.58	0.86	0.040	0.00		0.561				
YbCu ₂	40	0.17	0.62	0.12	0.03	0.14(8)	1.48	0.20	0.00	0.26(3)	0.94(2)
	60	0.23	0.62	0.14	0.03		1.40				
	80	0.20	0.58	0.14	0.03		1.26				
	100	0.27	0.55	0.16	0.03		1.23				
	120	0.24	0.58	0.16	0.03		1.16				
YbAl ₃	40	0.17	0.92	0.23	0.05	0.12(2)	7.35	0.15	0.00	0.025	0.79
	80	0.20	0.88	0.23	0.07		4.76				
	120	0.37	0.96	0.23	0.07		3.85				
Yb ₄ Sb ₃	40	0.17	0.83	0.040	0.000	0.25(8)	2.42	0.25	0.00	0.31(3)	0.58(2)
	80	0.20	0.78	0.040	0.00		0.950				
	120	0.24	0.78	0.040	0.00		0.770				
	140	0.46	0.75	0.040	0.00		0.499				
Yb ₄ Bi ₃	40	0.17	0.67	0.050	0.00	0.24(8)	0.996	0.25	0.00	0.29(3)	0.53(2)
	80	0.20	0.67	0.050	0.00		0.688				
	120	0.24	0.63	0.050	0.00		0.453				
	140	0.28	0.63	0.050	0.00		0.347				

a fit parameter, and the best values are listed in the fourth column of Table I. We see that the β value for the surface is smaller than for the bulk, which is physically reasonable.

Taking Γ , γ , α , β , $\epsilon_{f_{7/2}}^B$, and $\Delta E = \epsilon_{f_{7/2}}^S - \epsilon_{f_{7/2}}^B$ as adjustable parameters, we fit photoemission spectra of each Yb compound at several photon energies. For each compound the values of γ , α , $\epsilon_{f_{7/2}}^B$, ΔE are fixed the same at all photon energies, whereas Γ and β values are varied depending on the photon energy. The results of the fit are tabulated in Table I. The value of the surface core-level binding-energy shift (SCS) ΔE are listed in the last column. The identification of the surface peak as opposed to the bulk is made on the basis of (i) its rapid change with oxygen contamination and (ii) larger Gaussian broadening. The values of SCS range from 0.52 to 0.94 eV and the surface peaks are in the higher binding-energy side, similar to those of other rare-earth metals and Yb compounds reported so far.⁶⁻¹⁹

B. Core-level spectra of anion atoms

Figure 2 shows the core-level spectra of anion atoms (Pb 5*d*, Al 2*p*, In 4*d*, Sb 4*d*, and Bi 5*d*). The spectra were obtained by the same photoemission experiment as those of the 4*f* level of Yb atoms. These data were curve fitted by the same procedure as the Yb 4*f* spectra and the values of the parameters thus obtained are tabulated in Table II. In the curve fitting, we allowed the spin-orbit

splitting energy of the *d* or *p* levels and their relative intensities to be varied. These values also are shown in Table II, and they are in good agreement with atomic data. In the case of Pb 5*d* and Al 2*p* spectra, the raw data are fitted well with a single spin-orbit doublet component, showing no evidence of the surface shifted peaks. For the case of In 4*d*, Sb 4*d*, and Bi 5*d*, however, we need two sets of spin-orbit components to fit the data. Again we used the effect of contamination and the value of Γ to distinguish between the surface and bulk peaks. The sign and magnitude of the SCS ΔE , and their intensity ratio for the anion core level are also shown in Table II. We see that (i) the magnitudes of the SCS for anion core levels are similar to those of the Yb 4*f* level and (ii) the sign is the same as the Yb 4*f* case, i.e., the surface peak is in the high binding-energy side of the bulk peak. This is in contrast to the semiconductor cases,²⁴⁻²⁶ where cation and anion core levels have SCS's in the opposite directions. This implies that SCS's in these Yb metallic compounds are not due to the charge transfer as suggested by some models^{22,23} to explain SCS in semiconductors.

IV. DISCUSSIONS

A. Bulk 4*f* level positions

We can compare the bulk 4*f* level positions of each compound obtained from the above data analysis with those predicted by Johansson and Mårtensson's model.²⁰

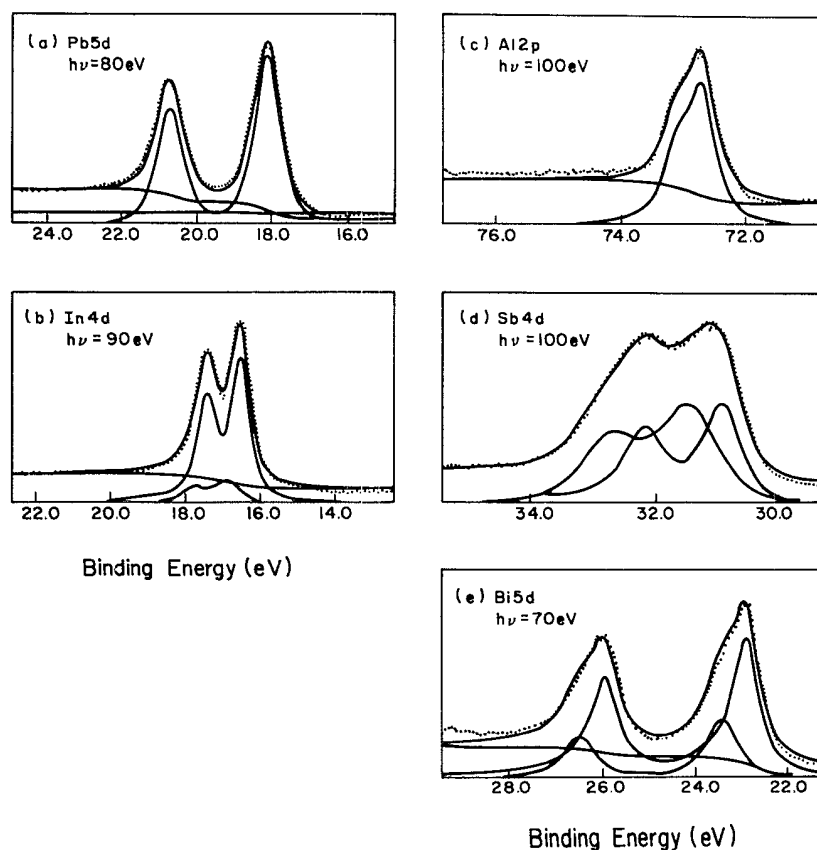


FIG. 2. Photoemission spectra of anion core levels (a) Pb 5*d*, (b) In 4*d*, (c) Al 2*p*, (d) Sb 4*d*, and (e) Bi 5*d*. By using either one spin-orbit splitting peak (Pb, Al) or two spin-orbit splitting peaks from the bulk and the surface (In, Sb, and Bi), we obtain the solid line by the least-squares curve fitting. The lower binding-energy peak represents the emission from the bulk and the higher binding-energy peak in some compounds (YbIn₂, Yb₄Sb₃, and Yb₄Bi₃) represents the emission from the surface.

TABLE II. Summary of the results from the analyses of the anion core-level photoemission spectra of YbPb₃, YbIn₂, YbAl₃, Yb₄Sb₃, and Yb₄Bi₃: 2Γ (FWHM) is the Gaussian broadening, β is the background ratio, 2γ (FWHM) is the Lorentzian broadening, I_S/I_B is the ratio of the peak intensities from the bulk and the surface atoms, α is the asymmetry parameter, $\epsilon_{d_{5/2}}^B$ ($\epsilon_{p_{3/2}}^B$) is the bulk binding energy of the $d_{5/2}$ ($p_{3/2}$) core level, and $\Delta E = \epsilon_{d_{5/2}}^S - \epsilon_{d_{5/2}}^B$ is the surface core-level energy shift. $\epsilon_{d_{3/2}} - \epsilon_{d_{5/2}}$ ($\epsilon_{p_{1/2}} - \epsilon_{p_{3/2}}$) is the spin-orbit splitting energy of the d (p) level, $I_{d_{3/2}}/I_{d_{5/2}}$ or $I_{p_{1/2}}/I_{p_{3/2}}$ is the intensity ratio of the two spin-orbit peaks. Estimated error bars are given in parentheses in units of the last digits.

Core levels	Photon energy (eV)	2Γ (eV)		β		2γ (eV)	I_S/I_B	α		$\epsilon_{d_{5/2}}^B$ ($\epsilon_{p_{3/2}}^B$) (eV)	$\Delta E = \epsilon_S - \epsilon_B$ (eV)
		B	S	B	S			B	S		
Pb 5d	80	0.60		0.10		0.34(4)		0.00		18.11(3)	
In 4d	90	0.33	0.57	0.070	0.00	0.38(4)	0.173	0.050	0.00	16.51(3)	0.36(2)
Al 2p	100	0.27		0.15		0.40(4)		0.00		72.49(3)	
Sb 4d	100	0.50	0.90	0.070	0.00	0.36(4)	1.16	0.10	0.00	30.90(3)	0.56(2)
Bi 5d	70	0.20	0.42	0.080	0.00	0.60(4)	0.398	0.10	0.00	22.89(3)	0.55(2)
		Spin orbit					Spin orbit				
$\epsilon_{d_{3/2}} - \epsilon_{d_{5/2}}$		2.62 eV for Pb 5d 0.90 eV for In 4d 1.25 eV for Sb 4d 3.04 eV for Bi 5d					$\epsilon_{p_{1/2}} - \epsilon_{p_{3/2}}$		0.40 eV for Al 2p		
$I_{d_{3/2}}/I_{d_{5/2}}$		0.69					$I_{p_{1/2}}/I_{p_{3/2}}$		0.50		

The basic assumption in this model is the fully screening valence charge distribution around the core-ionized site, and for the semiquantitative calculation they used a Born-Haber cycle to express the binding energy of the core level in terms of its binding energy in the gas phase and the difference of cohesive energies between the (Z) and ($Z+1$) element. Following this procedure and the Born-Haber cycle, we can write the binding energy of the divalent $4f$ level ($4f^{14} \rightarrow 4f^{13}$) in the compound ϵ_f^B (compound) as³¹

$$\begin{aligned} \epsilon_f^B(\text{compound}) = & \epsilon_f(\text{atom}) - I_A^* - E_{\text{coh}}^C(\text{Yb}^{3+}) \\ & + E_{\text{coh}}^C(\text{Yb}^{2+}) + E_{\text{imp}}^C(\text{Yb}^{3+}; \text{Yb}^{2+}), \end{aligned} \quad (1)$$

where $\epsilon_f(\text{atom})$ is the $4f$ ionization energy of the Yb atom, I_A^* is the neutralization energy, $E_{\text{coh}}^C(\text{Yb}^{3+})$ and $E_{\text{coh}}^C(\text{Yb}^{2+})$ are cohesive energies of the compound when the Yb atom is in the trivalent and divalent configuration, respectively, and $E_{\text{imp}}^C(\text{Yb}^{3+}; \text{Yb}^{2+})$ is the solution energy when one Yb atom is changed from trivalent configuration to divalent configuration. Here superscript B denotes the bulk value, and we neglect the effect of homogeneous mixed valency of the compound. Similarly, the binding energy of the $4f$ level ($4f^{14} \rightarrow 4f^{13}$) in Yb metal is written as follows:

$$\begin{aligned} \epsilon_f^B(\text{metal}) = & \epsilon_f(\text{atom}) - I_A^* - E_{\text{coh}}^M(\text{Yb}^{3+}) \\ & + E_{\text{coh}}^M(\text{Yb}^{2+}) + E_{\text{imp}}^M(\text{Yb}^{3+}; \text{Yb}^{2+}). \end{aligned} \quad (2)$$

Since the cohesive energies of the compound and the metal are related by the relation

$$E_{\text{coh}}^C = E_{\text{coh}}^M - \Delta H,$$

where ΔH is the heat of formation of the compound, we can write from Eqs. (1) and (2)

$$\begin{aligned} \Delta \epsilon_f^B & \equiv \epsilon_f^B(\text{compound}) - \epsilon_f^B(\text{metal}) \\ & = \Delta H(\text{Yb}^{3+}) - \Delta H(\text{Yb}^{2+}) - E_{\text{imp}}^M(\text{Yb}^{3+}; \text{Yb}^{2+}) \\ & \quad + E_{\text{imp}}^C(\text{Yb}^{3+}; \text{Yb}^{2+}) \end{aligned} \quad (3)$$

for the difference between the $4f$ level binding energy ($4f^{14} \rightarrow 4f^{13}$) in the Yb compound and that in the Yb metal.

Now the heat of formation ΔH and the heat of solution $E_{\text{imp}}^M(\text{Yb}^{3+}; \text{Yb}^{2+})$ can be estimated by the following Miedema's semiempirical equation:^{32,33}

$$\begin{aligned} E_{\text{imp}}^M(\text{Yb}^{3+}; \text{Yb}^{2+}) \\ = P \frac{V_{\text{Yb}}^{2/3}}{(n_{\text{WS}}^{-1/3})_{\text{av}}} \left[-\Delta\phi^* + \frac{Q}{P} (\Delta n_{\text{WS}}^{1/3})^2 \right], \end{aligned} \quad (4)$$

$$\begin{aligned} \Delta H(\text{Yb}) = & \frac{2f(c)}{(n_{\text{WS}}^{\text{Yb}})^{-1/3} + (n_{\text{WS}}^A)^{-1/3}} [C_{\text{Yb}} V_{\text{Yb}}^{2/3} + C_A V_A^{2/3}] \\ & \times P \left[-(\Delta\phi^*)^2 + \frac{Q}{P} (\Delta n_{\text{WS}}^{1/3})^2 - \frac{R}{P} \right], \end{aligned}$$

and

$$f(c) = C_{\text{Yb}}^S C_A^S [1 + 8(C_{\text{Yb}}^S C_A^S)^2],$$

$$C_{\text{Yb}}^S = \frac{C_{\text{Yb}} V_{\text{Yb}}^{2/3}}{C_{\text{Yb}} V_{\text{Yb}}^{2/3} + C_A V_A^{2/3}},$$

$$C_A^S = 1 - C_{\text{Yb}}^S,$$

where A represents the anion element, C_{Yb}, C_A are atomic concentrations, Yb denotes the divalent (Yb^{2+}) or

trivalent (Yb^{3+}) configuration, and $(P, Q/P, R/P)$ are constants and ϕ^* , $n_{\text{WS}}^{1/3}$, and V are parameters whose values depend on the Yb configuration and the anion element.^{32,33} Assuming Yb^{3+} (trivalent) $[\text{Xe}]4f^{13}5d6s^2$ ion is similar to Lu in terms of the valence electronic structure, we can obtain these parameter values easily from Ref. 32 by interpolation. These parameter values are written in Table III, and the heat of formation ΔH when Yb is in the Yb^{2+} (divalent) and Yb^{3+} (trivalent) configurations calculated using these parameters and $(P, Q/P, R/P)$ (Ref. 32) and Eq. (4) are given in Table IV. Here again the effect of homogeneous mixed valency has been ignored.

Now that we obtained $\Delta H(\text{Yb}^{3+})$ and $\Delta H(\text{Yb}^{2+})$ in Eq. (3), we need to know the values of $E_{\text{imp}}^M(\text{Yb}^{3+}:\text{Yb}^{2+})$ and $E_{\text{imp}}^C(\text{Yb}^{3+}:\text{Yb}^{2+})$ to compare with the experimental bulk $4f$ level positions of various Yb compounds. $E_{\text{imp}}^M(\text{Yb}^{3+}:\text{Yb}^{2+})$ can be calculated by Eq. (4) and parameters of Table III, and is found to be 49.54 KJ/mol (0.52 eV). The last term $E_{\text{imp}}^C(\text{Yb}^{3+}:\text{Yb}^{2+})$ is difficult to estimate, but there are good reasons to believe that it will be small.³¹ Hence this term will be assumed to be negligible here as in Ref. 31. The values of $\Delta\epsilon_f^B(\text{compound})$ thus obtained are listed in Table V for each compound, and compared with the experimental value using the known $4f$ level binding energy of Yb metal,^{9,10} $\epsilon_f^B(\text{metal})=1.25$ eV. We see that the predicted values of $\epsilon_f^B(\text{compound})$ shown in the second column agree with the measured ones shown in the third column very well in most compounds with the possible exceptions of YbCu_2 and Yb_4As_3 . This tells us that Johansson and Mårtensson's model reasonably describes the $4f$ level binding-energy positions even in these mixed-valent Yb compounds. The reason for the discrepancy in YbCu_2 and Yb_4As_3 is not clear, but most probably due to the nonnegligible $E_{\text{imp}}^C(\text{Yb}^{3+}:\text{Yb}^{2+})$ term for these compounds.

B. Surface core-level shifts of $4f$ levels

The $4f$ level binding energy from the surface atoms can be written as follows by the similar method for the bulk state:

$$\epsilon_f^S(\text{compound}) = \epsilon_f(\text{atom}) - I_x^* - E_{\text{coh}}^{S,C}(\text{Yb}^{3+}) + E_{\text{coh}}^{S,C}(\text{Yb}^{2+}) + E_{\text{imp}}^{S,C}(\text{Yb}^{3+}:\text{Yb}^{2+}),$$

TABLE III. Model parameter values for various divalent and trivalent metals which are used to calculate the heat of formation by Miedema's empirical scheme. Some parameters were taken from Refs. 32 and 33, and others were interpolated.

Metal	ϕ^* (V)	$n_{\text{WS}}^{1/3}(d.u.)^{1/3}$	$V_m^{2/3}$ (cm ²)
Yb^{2+}	2.70	0.98	8.40
$\text{Yb}^{3+}=\text{Lu}$	3.30	1.31	5.30
Pb	4.10	1.15	6.90
Al	4.20	1.39	4.60
In	3.90	1.17	6.30
Cu	4.55	1.47	3.70
As	4.80	1.44	5.20
Sb	4.40	1.26	6.60
Bi	4.15	1.16	7.20

TABLE IV. The heats of formation of intermetallic Yb compounds calculated by Miedema's scheme when Yb atoms are in the divalent and trivalent configurations.

Compound	$-\Delta H(\text{Yb}^{2+})$ kJ/mol (eV)	$-\Delta H(\text{Yb}^{3+})$ kJ/mol (eV)
YbPb_3	37.87 (0.39)	48.11 (0.50)
YbAl_3	15.37 (0.16)	60.95 (0.63)
YbAl_2	17.91 (0.19)	70.54 (0.73)
YbIn_2	30.56 (0.32)	52.88 (0.55)
YbCu_2	41.59 (0.43)	28.16 (0.29)
Yb_4As_3	62.62 (0.65)	140.6 (1.46)
Yb_4Sb_3	64.29 (0.67)	120.7 (1.26)
Yb_4Bi_3	55.25 (0.58)	97.50 (1.01)

where $E_{\text{coh}}^{S,C}(\text{Yb}^{3+})$ and $E_{\text{coh}}^{S,C}(\text{Yb}^{2+})$ are cohesive energies at the surface, and $E_{\text{imp}}^{S,C}(\text{Yb}^{3+}:\text{Yb}^{2+})$ is the solution energy when one trivalent Yb atom is dissolved into the divalent surface. Hence, the surface binding-energy difference between the compound and Yb metal is given by

$$\begin{aligned} \Delta\epsilon_f^S &= \epsilon_f^S(\text{compound}) - \epsilon_f^S(\text{metal}) \\ &= \Delta H^S(\text{Yb}^{3+}) - \Delta H^S(\text{Yb}^{2+}) - E_{\text{imp}}^{S,M}(\text{Yb}^{3+}:\text{Yb}^{2+}) \\ &\quad + E_{\text{imp}}^{S,C}(\text{Yb}^{3+}:\text{Yb}^{2+}), \end{aligned} \quad (5)$$

where superscript S at ΔH^S denotes the surface.

For the cohesive energies and the heat of solution, it was empirically found²⁰ that

$$E_{\text{coh}}^S = 0.8E_{\text{coh}}, \quad (6)$$

$$E_{\text{imp}}^{S,M}(\text{Yb}^{3+}:\text{Yb}^{2+}) = 0.8E_{\text{imp}}^M(\text{Yb}^{3+}:\text{Yb}^{2+})$$

because of the reduced number of neighboring atoms at the surface.

If we use this relation, Eq. (5) can be written as

$$\Delta\epsilon_f^S = 0.8\Delta\epsilon_f^B, \quad (7)$$

The calculated value of $\Delta\epsilon_f^S$ for each compound using the above equation is shown in the fourth column of Table V along with the experimental value in the fifth column using the experimental value^{9,10} of $\epsilon_f^S(\text{metal})=1.85$ eV. We see that the agreement between these two values is very reasonable for most compounds, the largest discrepancy being shown in YbCu_2 . But interestingly enough, even in YbCu_2 the discrepancy here is much smaller than that for the bulk $4f$ levels shown in the second and third columns of Table V. This points to the fact that the largest source of error in the theoretical predictions of Eq. (3) is the neglect of the $E_{\text{imp}}^C(\text{Yb}^{3+}:\text{Yb}^{2+})$ term as suggested earlier, since the relation Eq. (6) is most likely to hold for this heat of solution as well.

C. Anderson Hamiltonian parameters of bulk Yb compounds

It has been proposed that the electronic structures of anomalous Yb compounds can be described by the Anderson Hamiltonian as in the case of Ce compounds.¹⁸ The main differences between Yb and Ce compounds are

TABLE V. The bulk and the surface binding energies of Yb compounds relative to those of Yb metal calculated by the Johansson-Mårtensson's model are described in the text. These are compared with the experimental values obtained from our photoemission spectra.

Compound	$\Delta\epsilon_f^B = \epsilon_B(\text{compound}) - \epsilon_B(\text{metal})$ (eV)	Experiment ($\Delta\epsilon_f^B$) (eV)	$\Delta\epsilon_f^S = \epsilon_B^S(\text{compound}) - \epsilon_B^S(\text{metal})$ (eV)	Experiment ($\Delta\epsilon_f^S$) (eV)
YbPb ₃	-0.62	-0.55	-0.50	-0.61
YbAl ₃	-0.99	-1.05	-0.79	-0.86
YbAl ₂ ^a	-1.06	-1.01	-0.85	-0.69
YbIn ₂	-0.75	-0.70	-0.60	-0.78
YbCu ₂	-0.38	-0.99	-0.31	-0.65
Yb ₄ As ₃	-1.33	-0.91	-1.06	-0.86
Yb ₄ Sb ₃	-1.10	-0.90	-0.88	-0.92
Yb ₄ Bi ₃	-0.96	-0.91	-0.77	-0.98

^aReference 12.

that (i) the 4*f* hole in Yb compounds plays the role of 4*f* electron for Ce compounds (electron-hole symmetry), (ii) the value of 4*f* electron correlation energy U_{ff} is larger in Yb, and (iii) the value of the hybridization strength Δ between the 4*f* electron and the conduction band is smaller in Yb compounds. Trends (ii) and (iii) are expected from the lanthanide contraction of 4*f* wave functions, but it was found for YbAl₃ (Ref. 18) that the hybridization strength Δ is still big enough even for Yb compounds to control the physical properties. In this section we will use the *bulk* 4*f* features of the valence-band spectra to test how well the Anderson Hamilton prediction works for Yb compounds studied here and to obtain the hybridization strength Δ for each compound.

The lowest-order solution in the $1/N_f$ theory for the Anderson impurity Hamiltonian at zero temperature gives the following relations,³⁰

$$\frac{n_f}{1-n_f} = \frac{N_f \Delta}{\pi \epsilon_f}, \quad \chi_m(0) = \frac{\mu_{\text{eff}}^2 n_f}{3 \epsilon_f}, \quad (8)$$

where n_f is the number of 4*f* hole in Yb case, N_f represents the degeneracy of the 4*f* level in the ground state (which is taken to be 8 for Yb compounds because the value of spin-orbit splitting is 1.27 eV), Δ represents the hybridization strength between the 4*f* level and the

conduction band, ϵ_f represents the bulk 4*f* level binding energy which is equal to the Kondo temperature T_K in the spin-fluctuation limit, $\chi_m(0)$ is the magnetic susceptibility at zero temperature, and $\mu_{\text{eff}} = \sqrt{j(j+1)}g\mu_B$.

The number of the 4*f* hole n_f is equal to $v-2$, where v is the valence of the 4*f* electrons. The bulk valence v of Yb ions can be determined from the photoemission spectra by calculating the intensity ratio of the bulk 4*f* divalent peak $I_B(+2)$ and the bulk 4*f* trivalent peak $I_B(+3)$ using the relation^{34,35}

$$v = 2 + \frac{I_B(+3)}{\frac{13}{14}I_B(+2) + I_B(+3)}.$$

From a wide range valence-band photoemission spectra including the trivalent 4*f* peaks (not shown here), we deduced the valence of each Yb compound from this equation. The valence we obtained from our analyses are 2.10 for YbIn₂, 2.37 for Yb₄As₃, 2.20 for YbCu₂, 2.65 for YbAl₃, 2.39 for Yb₃Sb₃, 2.13 for Yb₄Bi₃ and 2.00 for YbPb₃ (divalent). These values are consistent with other photoemission results^{16,18,19} and lattice constant measurements.³⁶ Using these values of n_f and $\epsilon_{f7/2}^B$ listed in Table I, we obtain Δ and $\chi_m(0)$ for each compound using Eq. (8) and the results are summarized in Table VI along

TABLE VI. Anderson Hamiltonian parameters of Yb compounds along with the calculated and experimental zero-temperature susceptibility. Here n_f is the number of the 4*f* hole which is obtained from the experimentally determined valence v by the relation $v = 2 + n_f$, ϵ_f is the 4*f*_{7/2} level binding energy of the bulk, $\Delta = \pi\rho(\epsilon_f)V^2$ is the hybridization parameter, and $\chi_m(0)$ represents the magnetic susceptibility at zero temperature.

Compound	n_f	ϵ_f (meV)	Δ (meV)	$\chi_m(0 \text{ K}) \times 10^{-3}$ (emu/mol)	$\chi_m^{\text{exp}}(0 \text{ K}) \times 10^{-3}$ (emu/mol)
YbPb ₃	0	700			
YbAl ₃	0.65	25	18	6.0	4.6 ^a
YbIn ₂	0.10	550	24	0.041	0.070 ^a
YbCu ₂	0.18	260	22	0.16	0.17 ^a
YbAl ₂ ^b	0.40	240	63	0.37	0.41 ^a
Yb ₄ As ₃	0.37	300	69	0.28	
Yb ₄ Sb ₃	0.39	310	78	0.28	
Yb ₄ Bi ₃	0.13	290	17	0.10	

^aReference 36.

^bReference 12.

with the available experimental values of $\chi_m(0)$. We can see that the predicted value of $\chi_m(0)$ from the above relation is in good agreement with the available experimental value of $\chi_m^{\text{exp}}(0)$. This tells us that the Anderson Hamiltonian describes the electronic structure of Yb compound very well as in the case of Ce compounds. The value of hybridization strength Δ obtained from the above relation ranges from 17 to 78 meV. These values are smaller than most mixed-valent Ce compounds as expected from the lanthanide contraction of $4f$ wave functions, but still much larger than previously believed. Hence hybridization is considered to be important for understanding electronic structures of Yb compounds as well.

D. Mean free path of electrons

In Table I, we also list the intensity ratios of the surface and the bulk divalent $4f$ peaks at several different photon energies which were obtained as the results of the fit. From these values we can deduce the inelastic mean free path of electrons at different kinetic energies, which is of great fundamental and practical interest, in the following way. The probability of finding photoelectrons at the detector that are emitted from the depth z of the sample without losing energy can be written as

$$P(z, \theta) = P_0 \exp \left[-\frac{z}{l \cos \theta} \right],$$

where l is the electron mean free path and θ is the angle between the CMA analyzer and the normal direction of the sample, which is 42° in our experimental setup. If we assume that the surface of the sample is smooth and the surface layer of the thickness ΔS is purely divalent (which is reasonable since the binding energy of the surface shifted $4f$ peak is fairly deep), we can write

$$\begin{aligned} \frac{I_S(+2)}{I_B(+2)} &= \frac{\int_0^{\Delta S} \exp(-x/l \cos \theta) dx}{(3-v) \int_{\Delta S}^{\infty} \exp(-x/l \cos \theta) dx} \\ &= \frac{1}{3-v} [\exp(\Delta S/l \cos \theta) - 1], \end{aligned}$$

where $I_S(+2)$ and $I_B(+2)$ denote the intensity of the surface and the bulk divalent $4f$ peaks, respectively, and v is the bulk valence. Hence, the mean free path of the electron l can be obtained from the experimentally determined intensity ratio $I_S(+2)/I_B(+2)$ by the relation

$$\frac{l}{\Delta S} = \left[\cos 42^\circ \ln \left[1 + (3-v) \frac{I_S(+2)}{I_B(+2)} \right] \right]^{-1}.$$

Using the valence of each Yb compound as obtained above, we calculated values of $l/\Delta S$ at different kinetic energies and the results are shown in Fig. 3.

We note that the escape depth decreases monotonically with electron kinetic energy, and its minimum has not been reached at $\hbar\omega = 40$ eV. This deviation from the universal curve,³⁷ where the escape depth minimum occurs around the electron kinetic energy of 100 eV, has been noted before for heavy rare-earth metals and compounds.^{9,10,38} It is probably related to the fact that low-

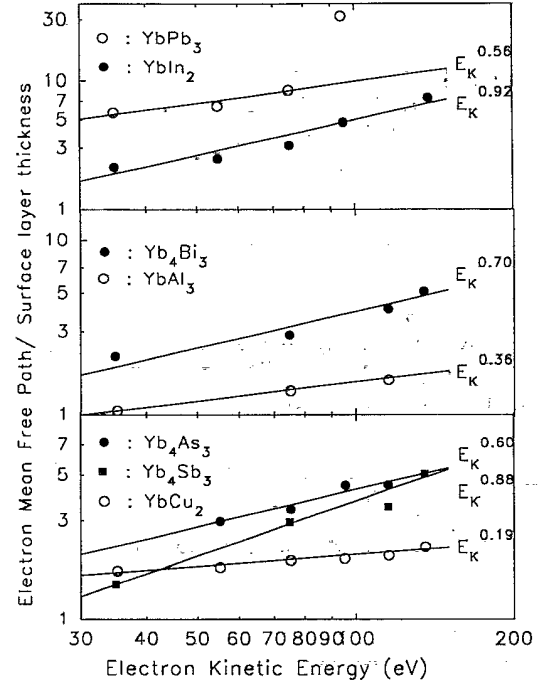


FIG. 3. Log-log plot of the mean free path of electrons divided by the divalent surface layer thickness ΔS as a function of the kinetic energy of electrons for (a) YbPb₃ and YbIn₂, (b) Yb₄Bi₃ and YbAl₃, (c) YbCu₂, Yb₄As₃, and Yb₄Sb₃.

energy excitation mechanisms exist for these compounds due to mixed-valency or heavy-fermion phenomena.^{31,39}

Various models propose that the asymptotic dependence of the electron mean free path l on its kinetic energy E_{kin} should have the form

$$\frac{l}{\Delta S} = \left[\frac{E_{\text{kin}}}{E_0} \right]^\delta + \text{const}, \quad (9)$$

where δ and E_0 are constants. Seah and Dench⁴⁰ proposed the δ value of 0.5, whereas Wagner, Davis, and Riggs⁴¹ deduced it as 0.65–0.75. In the log-log plot of $l/\Delta S$ relative to E_{kin} for each compound shown in Fig. 3, we find that Eq. (9) is reasonably well satisfied but the best value of δ depend on the compound ($\delta = 0.56$ in YbPb₃, 0.92 in YbIn₂, 0.88 in Yb₄Sb₃, 0.36 in YbAl₃, 0.60 in Yb₄As₃, 0.70 in Yb₃Bi₃, 0.19 in YbCu₂). Another interesting observation, when we compare Table I and Fig. 3, is that for compounds with larger β value (inelastic scattering coefficient) the mean free path l tends to be smaller (YbPb₃ seems to be an exception). This is intuitively reasonable, although more work needs to be done to deduce quantitative aspects.

V. CONCLUSIONS

Mixed-valent Yb compounds (YbIn₂, Yb₄As₃, YbCu₂, YbAl₃, Yb₄Sb₃, Yb₄Bi₃) and divalent YbPb₃ are studied by high-resolution photoemission spectroscopy using synchrotron radiation in the photon energy range $40 \leq \hbar\omega \leq 140$ eV. The SCS's (surface core-level binding-

energy shifts) are found in the $4f$ levels of all Yb compounds and the binding energies of surface atoms are found to be higher than those of bulk atoms. The SCS's ($\Delta E = \epsilon_S - \epsilon_B$) are 0.54 ± 0.02 eV in YbPb₃, 0.52 ± 0.02 eV in YbIn₂, 0.70 ± 0.02 eV in Yb₄As₃, 0.94 ± 0.02 eV in YbCu₂, 0.79 ± 0.02 eV in YbAl₃, 0.58 ± 0.02 eV in Yb₄Sb₃, and 0.53 ± 0.02 eV in Yb₄Bi₃. Also, for some Yb compounds (YbIn₂, Yb₃Sb₃, and Yb₃Bi₃) the SCS's of anion atom core levels are detected and the values are 0.36 ± 0.02 eV in In $4d$, 0.56 ± 0.02 eV in Sb $4d$, and 0.55 ± 0.02 eV in Bi $5d$. But the effects of surface atoms are not resolved for core levels of Al and Pb in our photoemission spectra of YbAl₃ and YbPb₃. These surface core-level shifts are reasonably well described by the Johansson and Mårtensson's fully screened core-hole model with Miedema's empirical scheme for cohesive energy estimation. The zero-temperature magnetic susceptibility $\chi(0)$ and the hybridization strength Δ between the $4f$ level and conduction electrons are also estimated us-

ing analytic relations for the Anderson impurity Hamiltonian with $U \rightarrow \infty$ from the $4f$ level binding energy and the Yb valence of these compounds obtained from the $4f$ level spectra, and the values of $\chi(0)$ are found to be consistent with the available experimental data and Δ is in the range of 17–78 meV. This shows that the Anderson impurity Hamiltonian is a good starting point for the description of electronic structures of Yb compounds. We also deduced the mean free path of electrons as a function of electron kinetic energy from the intensity ratios between the bulk and the surface atoms, and found that the mean free path on the electron kinetic energy can be reasonably fitted with the relation $l/\Delta S = (E_{\text{kin}}/E_0)^\delta + \text{const}$, although the value of δ depends on the compound.

ACKNOWLEDGMENT

This work was supported in part by the SNU Daewoo Research fund, Korea.

*Author to whom all correspondences should be addressed.

[†]Present address: Department of Material Physics, Faculty of Engineering Science, Osaka University, Toyonaka 560, Japan.

[‡]Present address: Department of Material Sciences, Faculty of Science, Hiroshima University, Hiroshima 730, Japan.

[§]Present address: Department of Physics, Faculty of Science, University of Tokyo, Hongo, Bunkyo-ku, Tokyo 113, Japan.

¹J. M. Lawrence, P. S. Riseborough, and P. D. Parks, *Rep. Prog. Phys.* **44**, 1 (1981).

²G. R. Stewart, *Rev. Mod. Phys.* **56**, 755 (1984).

³J. W. Allen, S.-J. Oh, O. Gunnarsson, K. Schönhammer, M. B. Maple, M. S. Torikachivili, and I. Lindau, *Adv. Phys.* **35**, 275 (1986).

⁴N. E. Bickers, D. L. Cox, and J. W. Wilkins, *Phys. Rev. Lett.* **54**, 230 (1985); *Phys. Rev. B* **36**, 2036 (1987).

⁵C. Laubschat, E. Weschke, C. Holtz, M. Domke, O. Strebler, and G. Kaindl, *Phys. Rev. Lett.* **65**, 1639 (1990).

⁶R. Kammerer, J. Barth, F. Gerken, A. Flodstrom, and L. I. Johansson, *Solid State Commun.* **41**, 435 (1980).

⁷G. Kaindl, C. Laubschat, B. Reihl, R. A. Pollak, N. Mårtensson, F. Holtzberg, and D. E. Eastman, *Phys. Rev. B* **26**, 1713 (1982).

⁸W. Gudat, M. Campagna, R. Rosei, J. H. Weaver, W. Eberhardt, F. Halliger, and E. Kaldis, *J. Appl. Phys.* **52**, 2123 (1981).

⁹S. F. Alvarado, M. Campagna, and W. Gudat, *J. Electron Spectrosc. Relat. Phenom.* **18**, 13 (1980).

¹⁰M. H. Hecht, A. J. Viescas, I. Lindau, J. W. Allen, and L. I. Johansson, *J. Electron Spectrosc. Relat. Phenom.* **34**, 343 (1984).

¹¹Y. Takokuwa, S. Takahashi, S. Suzuki, S. Kono, T. Yokotsuko, T. Takahashi, and T. Sagawa, *J. Phys. Soc. Jpn.* **51**, 2045 (1982).

¹²G. Kaindl, B. Reihl, D. E. Eastman, R. A. Pollak, N. Mårtensson, B. Barbara, T. Penny, and T. S. Plaskett, *Solid State Commun.* **41**, 157 (1982).

¹³M. Domke, C. Laubschat, E. V. Sampathkumaran, M. Prietsch, T. Mandel, G. Kaindl, and H. U. Middelmann, *Phys. Rev. B* **32**, 8002 (1985).

¹⁴G. K. Wertheim, J. H. Wernick, and G. Crecelius, *Phys. Rev. B* **18**, 878 (1978).

¹⁵L. I. Johansson, A. Flodstrom, S.-E. Hornstom, B. Johansson, J. Barth, and F. Gerken, *Solid State Commun.* **41**, 427 (1982).

¹⁶A. Fujimori, T. Shimizu, and H. Yasuoka, *Phys. Rev. B* **35**, 8945 (1987).

¹⁷S. Ogawa, A. Fujimori, S. Suga, M. Taniguchi, M. Fujisawa, T. Shimizu, H. Yasuoka, and K. Yoshimura, *Solid State Commun.* **67**, 1093 (1988).

¹⁸S.-J. Oh, S. Suga, A. Kakizaki, M. Taniguchi, T. Ishii, J.-S. Kang, J. W. Allen, O. Gunnarsson, N. E. Christensen, A. Fujimori, T. Suzuki, T. Kasuya, T. Miyahara, H. Kato, K. Schönhammer, M. S. Torikachivilli, and M. B. Maple, *Phys. Rev. B* **37**, 2861 (1988).

¹⁹S. Suga, S. Ogawa, H. Namatame, M. Taniguchi, A. Kakizaki, T. Ishii, A. Fujimori, S.-J. Oh, H. Kato, T. Miyahara, A. Ochiai, T. Suzuki, and T. Kasuya, *J. Phys. Soc. Jpn.* **58**, 4534 (1989).

²⁰B. Johansson and N. Mårtensson, *Phys. Rev. B* **21**, 4427 (1980).

²¹P. H. Citrin and G. K. Wertheim, *Phys. Rev. B* **27**, 3137 (1983).

²²J. W. Davenport, R. E. Watson, M. L. Perlman, and T. K. Sham, *Solid State Commun.* **40**, 999 (1981).

²³C. Priester, G. Allan, and M. Lannoo, *Phys. Rev. Lett.* **58**, 1989 (1987).

²⁴D. E. Eastman, T.-C. Chiang, P. Heimann, and F. J. Himpsel, *Phys. Rev. Lett.* **45**, 656 (1980).

²⁵Taniguchi, S. Suga, M. Seki, K. L. I. Kobayashi, and H. Kan-zaki, *J. Phys. C* **16**, L45 (1983).

²⁶T. Kendelewicz, P. H. Mabowald, K. A. Bertness, C. E. McCants, I. Lindau, and W. E. Spicer, *Phys. Rev. B* **36**, 6543 (1987).

²⁷T. Miyahara, S. Suzuki, T. Hanyu, H. Kato, K. Naito, H. Fukutai, I. Nakakura, H. Sugawara, S. Nakai, T. Ishii, H. Noda, T. Namioka, and T. Sasaki, *Jpn. J. Appl. Phys.* **24**, 293 (1985).

²⁸G. D. Mahan, *Phys. Rev. B* **11**, 4812 (1975).

²⁹S. Doniach and M. Sunjic, *J. Phys. C* **3**, 285 (1970).

³⁰Y. Kuramoto and E. Müller-Hartmann, *J. Magn. Magn. Mater.* **52**, 122 (1985).

³¹C. Laubschat, G. Kaindl, W.-D. Schneider, B. Reihl, and N. Mårtensson, *Phys. Rev. B* **33**, 6675 (1986).

- ³²A. R. Miedema, P. F. de Châtel, and F. R. de Boer, *Physica B* **100**, 1 (1980).
- ³³A. R. Miedema, *J. Less-Common Met.* **46**, 167 (1976).
- ³⁴S.-J. Oh, J. W. Allen, M. S. Torikachivili, and M. B. Maple, *J. Magn. Magn. Mater.* **52**, 183 (1985).
- ³⁵We believe the relation in Ref. 16 is slightly in error because it neglects the degeneracy ratio 13/14.
- ³⁶J. C. P. Klaasse, F. R. de Boer, and P. F. de Châtel, *Physica B* **106**, 178 (1981).
- ³⁷I. Lindau and W. E. Spicer, in *Synchrotron Radiation Research*, edited by H. Winick and S. Doniach (Plenum, New York, 1980), p. 159.
- ³⁸S.-J. Oh and J. W. Allen, *Phys. Rev. B* **30**, 1937 (1984).
- ³⁹D. R. Penn, *Phys. Rev. B* **13**, 5248 (1976).
- ⁴⁰M. P. Seah and W. A. Dench, *Surf. Interface Anal.* **1**, 2 (1979).
- ⁴¹C. D. Wagner, L. E. Davis, and M. Riggs, *Surf. Interface Anal.* **2**, 53 (1980).